Rational Design of Charge-Neutral, Near-Infrared-Emitting Osmium(II) Complexes and OLED Fabrication

ARTICLE *in* ADVANCED FUNCTIONAL MATERIALS · AUGUST 2009

Impact Factor: 11.81 · DOI: 10.1002/adfm.200900233

9 AUTHORS, INCLUDING:

Yun Chi
National Tsing Hua University
342 PUBLICATIONS **10,797** CITATIONS
SEE PROFILE

Chung-Chia Chen
National Taiwan University
22 PUBLICATIONS **685** CITATIONS
SEE PROFILE

Chih-Hao Chang
Yuan Ze University
69 PUBLICATIONS **1,785** CITATIONS
SEE PROFILE

Rational Design of Charge-Neutral, Near-Infrared-Emitting Osmium(II) Complexes and OLED Fabrication

By *Tsang-Chi Lee, Jui-Yi Hung, Yun Chi,* Yi-Ming Cheng, Gene-Hsiang Lee, Pi-Tai Chou,* Chung-Chia Chen, Chih-Hao Chang,* and *Chung-Chih Wu**

A new series of charge neutral Os(II) isoquinolyl triazolate complexes (1–4) with both *trans* and *cis* arrangement of phosphine donors are synthesized, and their structural, electrochemical and photophysical properties are established. In sharp contrast to the *cis*-arranged complexes 2–4, the *trans* derivative 1, which shows a planar arrangement of chromophoric *N*-substituted chelates, offers the most effective extended π-delocalization and hence the lowest excited state energy gap. These complexes exhibit phosphorescence with peak wavelengths ranging from 692–805 nm in degassed CH_2Cl_2 at room temperature. Near-infrared (NIR)-emitting electroluminescent devices employing 6 wt % of 1 (or 4) doped in Alq_3 host material are successfully fabricated. The devices incorporating 1 as NIR phosphor exhibit fairly intense emission with a peak wavelength at 814 nm. Forward radiant emittance reaches as high as 65.02 $\mu W\,cm^{-2}$, and a peak EQE of ~1.5% with devices employing Alq_3, TPBi and/or TAZ as electron-transporting/exciton-blocking layers. Upon switching to phosphor 4, the electroluminescence blue shifts to 718 nm, while the maximum EQE and radiance increase to 2.7% and 93.26 ($\mu W\,cm^{-2}$) respectively. Their performances are optimized upon using TAZ as the electron transporting and exciton-blocking material. The OLEDs characterized represent the only NIR-emitting devices fabricated using charge-neutral and volatile Os(II) phosphors via thermal vacuum deposition.

1. Introduction

Transition metal complexes showing strong phosphorescent emission at room temperature (RT) have received a great deal of attention in recent years due to their rich photophysical properties[1] and potentials for fabricating the organic light emitting diodes (OLEDs) suited for full color displays, or white-light OLEDs applicable to general-purpose lighting as well as for backlights of liquid crystal displays.[2] The majority of reported phosphors exhibit emission in the typical visible range from sky-blue to saturated-red. In recent days, however, room temperature true-blue phosphorescence with peaks centered around 460 nm also has been achieved upon employing benzyl substituted carbene or phosphine chelate, together with the large-gap pyridyl azolates as the chromophoric chelates.[3] Relative to other weakly emitting blue phosphors, the enhanced true-blue emission can be rationalized by the exceedingly strong metal-ligand bonding character exerted by the benzyl substituted ancillary chelates that destabilize the metal-centered dd excited states[4] as well as the effective blocking of the unwanted ligand-to-ligand charge transfer transition that commonly acts as the non-radiative quenching channel.[5] Consequently, true-blue OLEDs with satisfactory efficiencies were fabricated upon employing device architectures with double-emitting layers and better confinement of both excitons and carriers.[6]

Parallel to the studies aimed at the design of shorter-wavelength, true-blue phosphors,[3] other groups have been focusing on the preparation of phosphors showing luminescence with peak wavelength longer than 700 nm, i.e., in the near infrared (NIR) region,[7] which is important for applications in the fields of signaling, night vision, telecommunication and wound healing, etc. Some strategies for NIR emission comprise employment of the donor-acceptor organic dyes, conjugated oligomers[8] as well as the heteroleptic Ir(III) cyclometalates,[9] while the alternative approach involves utilization of intermolecular $\pi\pi$ stacking occurring in the solid state. The latter has been documented for Pt(II) metal complexes that possess planar geometry. As such, many efficient NIR-emitting OLEDs based on these Pt(II)

[*] Prof. Y. Chi, T.-C. Lee, J.-Y. Hung
Department of Chemistry
National Tsing Hua University
Hsinchu 300 (Taiwan)
E-mail: ychi@mx.nthu.edu.tw
Prof. P.-T. Chou, Dr. Y.-M. Cheng, Dr. G.-H. Lee
Department of Chemistry and Instrumentation Center
National Taiwan University
Taipei 106 (Taiwan)
E-mail: chop@ntu.edu.tw
Prof. C.-C. Wu, C.-C. Chen, C.-H. Chang
Department of Electrical Engineering
Graduate Institute of Photonics and Optoelectronics and
Graduate Institute of Electronics Engineering
National Taiwan University
Taipei 106 (Taiwan)
E-mail: chungwu@cc.ee.ntu.edu.tw

DOI: 10.1002/adfm.200900233

complexes were demonstrated.[8a,10] Most notably, NIR devices with electroluminescence at $\lambda = 772$ nm and maximum external quantum efficiency (EQE) of over 8.5% have been reported for the tetrabenzoporphyrin Pt(II) phosphor in 4,4′-bis(*N*-carbazolyl)biphenyl (CBP) and with 2,9-dimethyl-4,7-diphenyl-1,10-phenanthroline (BCP) as an exciton blocking (EBL) and electron transport layer (ETL).[11]

In this article, as the continuation of our efforts to develop efficient phosphorescent materials for OLED applications,[12] we report new Os(II) complexes with highly conjugated isoquiniolinyl triazolate chelate to obtain phosphors that shine at the longer wavelength region. It is particularly notable that these Os(II) phosphors use their lower energy MLCT contribution to further red shift the emission. This is sharply in contrast to the above mentioned square planar Pt(II) complexes that typically employed the intermolecular $\pi\pi$ stacking interaction to lower the emission gap. Note that the respective packing formation never exists for Os(II) metal complexes due to their octahedral configuration. Finally, although there are quite a few NIR-emitting Os(II) and Ru(II) based analogues documented in recent literature,[7c,13] our complexes presented in this study are charge-neutral and volatile, making them ideal for the device fabrication employing thermal vacuum deposition.

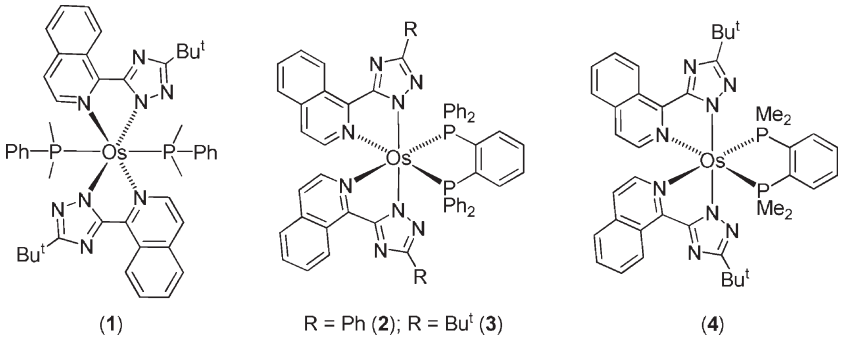

Scheme 1. Structural drawing of complexes **1**–**4**.

2. Results and Discussion

2.1. Synthesis and Characterization

As mentioned earlier,[14] the carbonyl reagent $Os_3(CO)_{12}$ is capable of reacting with a variety of 2-pyridyl azoles in diethylene glycol monomethyl ether (DGME) solution, giving rise to the *cis*-dicarbonyl complexes $[Os(CO)_2(N^\wedge N)_2]$, for which N^N chelates represent the pyridyl azolate chelates employed. Upon further treatment with freshly sublimed Me_3NO, followed by addition of two equiv. of monodentate phosphine, the *trans*-substituted complexes $[Os(N^\wedge N)_2P_2]$ can be isolated in moderate to good yields.[14] Moreover, the reactions with CF_3 functionalized azoles render better yields than those employing methyl or *t*-butyl substituted azoles, showing that the reactivity is somewhat governed by the acidity of the azolic N-H group.

Since our goal in the present article is to evaluate phosphors with emission occurring in the longer wavelength range of $\geq$800 nm, the more conjugated 5-(1-isoquinolyl)-1,2,4-triazoles were selected in all current investigations for lowering the excited state energy gap. Moreover, three phosphine ligands, namely: dimethylphenylphosphine, 1,2-bis(diphenylphosphino)benzene (dppb) and 1,2-bis(dimethylphosphino)benzene (dmpb), were employed for studying the influence related to their electronic characters and effect exerted by the accompanied geometrical isomerism. The respective synthetic procedures render four charge neutral, isoquinolyl triazolate Os(II) complexes (**1**–**4**) in moderate yields (Scheme 1). Although their molecular structures seem somewhat identical to our previously reported Ru(II) congeners,[15] it should be noted that their basic electrochemical, photophysical and thermodynamic characteristics are significantly different. First of all, all Os(II) metal complexes discussed in this manuscript are chemically more stable than the respective Ru(II) complexes.[15b] This is mainly due to the improved metal-ligand bonding interaction and enhanced ligand field strength associated with the third-row metal elements. Secondly, all Os(II) complexes have showed much bathochromic shifted phosphorescence and lower electrochemical oxidation potential compared with their second-row, Ru(II) congeners. As a result, they are expected to serve as appropriate NIR emitters with improved device efficiencies. Detailed characterization, spectral data and analyses as well as devices fabrication and performance are elaborated in the following sections.

2.2. X-Ray Crystallography

Figure 1 depicts the molecular structure of complex **4**, showing a mandated *cis*-P,P arrangement and a relaxed P–Os–P bite angle of

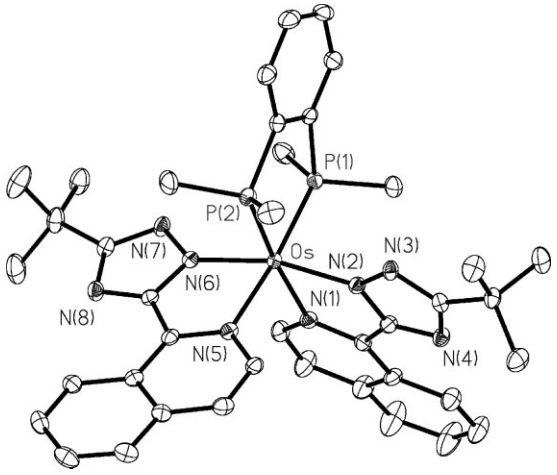

Figure 1. ORTEP diagram of complex **4** with thermal ellipsoids shown at 30% probability level. Selected bond distance and angles: Os–N(1) = 2.145(3), Os–N(2) = 2.059(2), Os–N(5) = 2.138(3), Os–N(6) = 2.056(2), Os–P(1) = 2.2518(8), Os–P(2) = 2.2546(8) Å and $\angle$ P(1)-Os-P(2) = 84.83(3)°.

Table 1. Photophysical and electrochemical properties for complexes **1**–**5**.

	photophysical properties [a]					$E_{1/2}$(V) [ΔE_p (mV)][b]	
	abs. λ_{max} ($\varepsilon \times 10^3$) $M^{-1}cm^{-1}$	PL λ_{max} (nm)	Φ (%)	τ (μs)	$k_r \times 10^5$ (s^{-1})	oxidation $E_{1/2}$	reduction $E_{1/2}$
1	321(40), 351(19), 468 (33), 552 (4.8), 694 (2.2)	805	0.2	0.04	0.5	−0.35 [94]	−2.50 [90] −2.93 [110]
2	309 (47), 319 (41), 340 (32), 357 (29), 410 (13), 482 (5.3), 568 (1.9)	692	15	0.76	1.98	0.08 [90]	−2.32 [90] −2.53 [90]
3	305 (28), 341 (18), 355 (19), 410 (11), 481 (4.5), 569 (1.5)	695	8	0.68	1.18	0.02 [130]	−2.40 [80] −2.63 [80]
4	307 (25), 342 (16), 356 (16), 418 (8.5), 493 (3.6), 583 (2.0)	731	4	0.16	2.54	−0.11 [80]	−2.38 [90] −2.60 [90]

[a] Samples were degassed and recorded in CH_2Cl_2 at RT with ε in $M^{-1}cm^{-1}$. [b] All electrochemical potentials were measured in a 0.1 M $TBAPF_6/CH_2Cl_2$ and THF solution for oxidation and reduction reaction, and reported in volts using Fc/Fc^+ as reference (0.53 V); ΔE_p is defined as E_{ap} (anodic peak potential) – E_{cp} (cathodic peak potential) and these data are quoted in mV. The Pt electrode and Au(Hg) alloy were selected as the working electrode of oxidation and reduction processes, respectively.

84.83(3)° for the dmpb chelate. The 5-(1-isoquinolyl)-3-*tert*-butyl-1,2,4-triazole (ibtz) chromophores adopt an eclipse orientation with both triazolate nitrogen atoms N(2) and N(6) aligned *trans* to each other, and with the isoquinolyl nitrogen atoms N(1) and N(5) located *trans* to the chelating phosphorus atoms. The adoption of *cis*-P,P arrangement in **4** has notably improved the Os-P bond strength. This is confirmed by a reduction of averaged Os-P distance from 2.362 Å in the *trans*-P,P complex $[Os(fppz)_2(PPh_2Me)_2]$ to ≈2.253 Å in **4**, along with an increase of the Os–$N_{(py)}$ bonding from 2.090 Å in $[Os(fppz)_2(PPh_2Me)_2]$ to a longer Os-$N_{(iq)}$ distance of 2.142 Å in **4**, while leaving the *trans* Os–$N_{(tz)}$ distances unaltered; 2.073 Å in $[Os(fppz)_2(PPh_2Me)_2]$ versus 2.058 Å observed in **4**.[14] The $N_{(iq)}$ atoms in **4** are located opposite to the more π-accepting *cis*-P,P atoms; thus, the increase of Os–$N_{(iq)}$ bond distances is presumably caused by the much greater *trans*-effect of phosphine, while the concomitant strengthening of Os-P bonding may also reduce the electron density on metal center, giving an increase of its HOMO/LUMO energy gap and a blue-shifting of emission peak wavelength versus the *trans*-analogues. The observed chelating ligand/structural dependence is akin to the respective *cis*-Ru(II) isoquinolyl complexes reported earlier in literature.[15]

2.3. Photophysical and Electrochemical Properties

As shown in both Table 1 and Figure 2, the sharp absorption band observed around 468 nm for **1** is assigned to the spin-allowed $^1\pi\pi^*$ transition mainly associated with the isoquinolyl-triazolate chelates chelating chromophores. The next lower energy absorption band around 552 nm is ascribed to a spin-allowed metal-to-ligand charge transfer (^{1}MLCT) transition, while the much broadened absorption band at the longest wavelength can reasonably be assigned to a mixed state involving both spin-orbit coupling enhanced $^3\pi\pi^*$ and ^{3}MLCT transitions. In good agreement with these descriptions, the $T_1 \rightarrow S_0$ transition (phosphorescence) of **1** occurring at 805 nm (c.f. Fig. 3) should possess substantial contribution from both spin-forbidden $\pi\pi^*$ and MLCT characters.

For further comparison, the UV/Vis spectra of complexes **2**–**4** are also depicted in Figure 2. It is obvious that complex **2** gave much intense absorption bands in the higher energy region 309–357 nm. This could be due to the fact that its 5-(1-isoquinolyl)-3-phenyl-1,2,4-triazole (iptz) ligand possesses an unsaturated phenyl group rather than the *tert*-butyl substituent, and hence provides stronger light harvesting character versus its counterparts **3** and **4**. The next lower energy absorptions centered at ≈410 nm are assigned to the ligand-centered $^1\pi\pi^*$ transition associated with the whole isoquinolyl-triazolate chelates. In good agreement with the

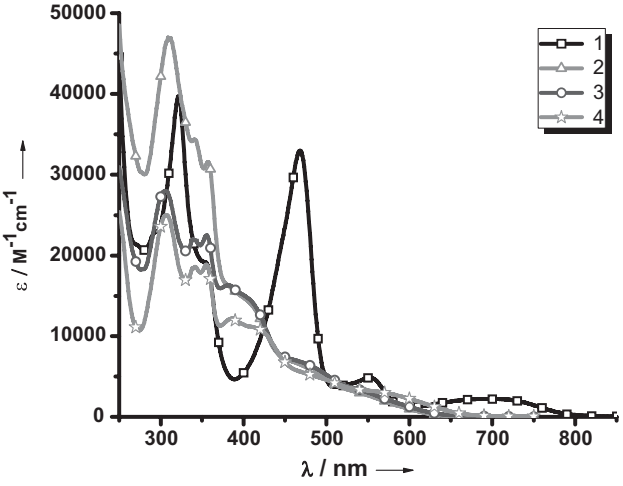

Figure 2. UV-Vis absorption spectra of complexes **1**–**4** in a CH_2Cl_2 solution at room temperature.

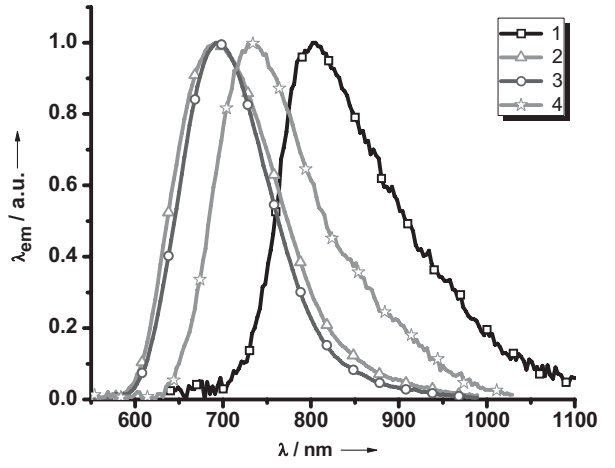

Figure 3. The normalized emission spectra of various Os(II) complexes in a CH_2Cl_2 solution at room temperature.

crystallographically determined *cis*-geometry for **2–4** (vide supra), the mutually perpendicular arrangement of chelating chromophores may destabilize the LUMO energy of the isoquinolyl moiety, and hence the blue shift of $\pi\pi^*$ transition (≈410 nm) relative to that of complex **1** (≈468 nm). At > 450 nm, strong spectral overlaps occurred among singlet MLCT and the corresponding ^{3}MLCT and $^3\pi\pi^*$ transitions, the result of which hampered definitive identification of their spectral positions. With respect to that of dppb derivatives **2** and **3**, the dmpb substituted **4** exhibits a much enhanced extinction coefficient as well as substantial bathochromic shifts for the lowest energy absorption peak. We speculate that dmpb chelate, with better electron donating strength, is capable to increase the spin-orbit coupling, resulting in an increase of extinction coefficient as well as a substantial reduction of the MLCT transition energies. This viewpoint is also supported by the largest radiative phosphorescence decay rate, k_r (see Table 1), for **4** and hence the strongest $T_1 \rightarrow S_0$ transition among **2–4**.

Figure 3 depicts the emission spectra of **1–4** in deoxygenated CH_2Cl_2. In accordance with the absorption spectra, the emission of **2–4** also occurred at the higher energy region than that of **1**. In all cases, drastic O_2 quenching of the emission intensity and structureless peak profiles are suggestive of the emission originating from the triplet manifold, i.e., phosphorescence, the transition of which possibly possesses a greater portion of MLCT versus $\pi\pi^*$ character. Accordingly, the rate of $S_1 \rightarrow T_n$ intersystem crossing should be fast and the $T_1 \rightarrow S_0$ transition should be partially allowed due to strong spin-orbit coupling and hence great state mixing between singlet and triplet manifolds. The latter is evidenced by phosphorescence radiative rate constants of $\approx 1 \times 10^5\ s^{-1}$ for all complexes **1–4**, which are either compatible or relatively larger than many other Os(II) complexes.[16] More discussion will be elaborated in the section of theoretical approaches. From the spectrum point of view, the emission peak maxima λ_{max} for **2** and **3** are essentially identical, revealing the stronger influence exerted by the phosphine chelate rather than from the substituent of triazolate fragment. Moreover, due to the planarity and hence elongation of the π-electron conjugation (vide supra), complex **1** reveals longest NIR emission. This is also indicated by the smallest k_r value ($0.5 \times 10^5\ s^{-1}$) for **1**, consistent with theoretical prediction, stating that in a homogeneous medium, the radiative, i.e., spontaneous, decay rate constant is inversely proportional to the third power of emitting wavelength.

Supplementary supports of the above mentioned emission spectral properties and rationalization are rendered via the computational approaches. Theoretical confirmation of the underlying basis for the photophysical properties of the studied complexes was provided by the density functional theory (DFT) MO calculations. With the use of the TD-B3LYP method incorporating B3LYP/LANL2DZ and 6-31G* optimized T_1 state geometry, together with the continuum PCM solvation model (see Experimental Section), the vertical (i.e., Franck–Condon) excitation energy from the ground-state to lowest lying triplet state was calculated. For all four complexes, as listed in Table 2, the calculated lowest lying $T_1 \rightarrow S_0$ transitions match well with respect to the experimental results. For example, the T_1 state of **1** is calculated to be around ≈890 nm, the value of which is close to the peak maximum of ≈805 nm of the emission spectrum recorded in CH_2Cl_2 solution. Furthermore, the calculated energy gaps of T_1 states of **2** (797 nm), **3** (790 nm), and **4** (805 nm) are also qualitatively in agreement with the peak maxima of their emission spectra recorded in a CH_2Cl_2 solution (see Table 1). These results indicate the TDDFT calculation works well in predicting the Franck–Condon transition for phosphorescence of **1–4**. In fact, the results also correctly predict that the phosphorescence emission in terms of peak wavelength should be in the order of **1** < **4** < **2** ≈ **3**, in good agreement with the experimental data.

Table 2. The calculated energy levels and orbital transition analyses of the studied Os(II) complexes.

	λ_{cal} (nm)	assignments	MLCT (%)
1	895.2	HOMO → LUMO (+100%)	59.39
2	797.5	HOMO → LUMO (+100%)	48.19
3	790.1	HOMO → LUMO (+98%)	53.64
4	805.4	HOMO → LUMO (+97%)	55.53

Figures 4 depicts the HOMO and LUMO frontier orbitals together with their energy diagram that are mainly involved in the $T_1 \rightarrow S_0$ transitions. The orbital descriptions and the energy gaps for all four complexes are listed in Table 2. The data of computational approaches compiled in Figure 4 and Table 2 can be summarized into several remarks. First, the excitations of the lowest triplet states (T_1) of complexes **1–4** are primarily attributed to HOMO → LUMO transition. Secondly, the HOMO of **1** is mainly contributed by the central metal atom and the two triazolate moieties, while its LUMO is mainly delocalized at the two isoquinolinyl fragments. The result is suggestive of an MLCT ($d_\pi(Os) \rightarrow \pi^*$ transition) mixed with an ILCT/LLCT transition. On the contrary, the transition, in the cases of **2–4**, is primarily ascribed to MLCT mixed with a relatively more localized $\pi\pi^*$ transition (ILCT) because its HOMO and LUMO are mainly distributed in the central metal atom and only one of the triazolate isoquinolinyl segments. In comparison to **2–4**, the more delocalized frontier orbital of **1** may imply an increasing probability of solvent quenching, which is consistent with the larger nonradiative rate constant compared to that of **2–4**. For example, the nonradiative

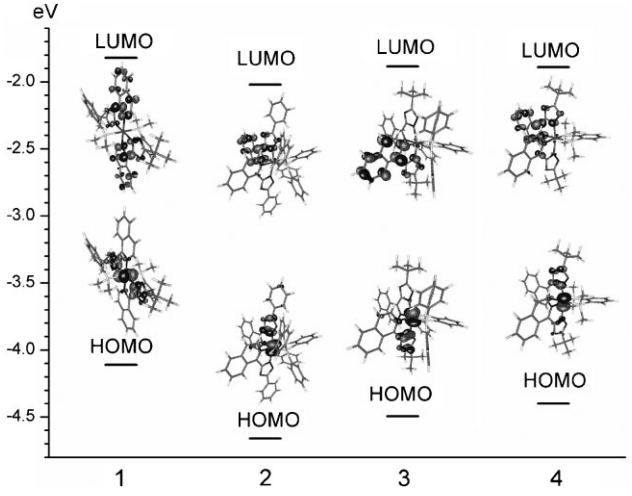

Figure 4. The HOMO and LUMO of complexes **1–4** on the basis of the T_1 state structural optimized geometries.

rate constant of **1** estimated from the quantum yield and the observed lifetime is about $2.5 \times 10^7\ s^{-1}$, while it is nearly one-twentieth of **1** in the case of complex **2** ($1.3 \times 10^6\ s^{-1}$). Additionally, as shown in Table 2, the spectacularly large MLCT percentages (≈50%) of complexes **1**–**4** correlate well with large radiative rate constants resolved experimentally (vide supra, see Table 1). Finally, as indicated in Figure 4, the relatively higher HOMO of **1** in terms of energy as compared to **2**–**4** is tentatively ascribed to the elongated conjugation length, as a consequence of the mediation by the d_π-orbital on the central metal Os(II) atom and the two nearly coplanar triazolate moieties. On the other hand, the elongation of the conjugation length does not occur in LUMO because the d_π-orbital has negligible contribution. As a result, the orbital energy of LUMO of **1** is not decreased as compared to **2**–**4** even though the extent of distribution of the π electron densities is also as significant as HOMO of **1**.

The redox potentials of all complexes were determined from cyclic voltammetry, for which the data are summarized in both Table 1 and Figure 5. It is believed that the oxidation mainly occurred at the Os(II) center, together with minor contributions from the N^N chelate and ancillary phosphines. Accordingly, complex **1** gives the lowest oxidation potential at −0.35 V, while **4** exhibits the second lower oxidation peak at −0.11 V due to the employment of two PMe_2Ph ligands as well as the dmpb chelate, both are expected to increase the relative electron density at the metal atom. Moreover, slightly more positive potential for **2** (0.08 V) and **3** (0.02 V) was also observed, which is attributed to the stronger electron accepting dppb chelate, while the small variation is apparently caused by the phenyl substituent versus the *tert*-butyl group on triazolate fragments.

As for the reduction behavior, complex **1** exhibits two reduction peaks at −2.50 and −2.93 V, a result being consistent with the fully delocalized N^N chelates. In sharp contrast, all other complexes exhibit less negative reduction couples; one is at the more positive range −2.32 to −2.40 V, while the other appeared at the range of −2.53 to −2.60 V. It appears to us that the reduction mainly occurs at each individual N^N chelate, while substituent at the azolate

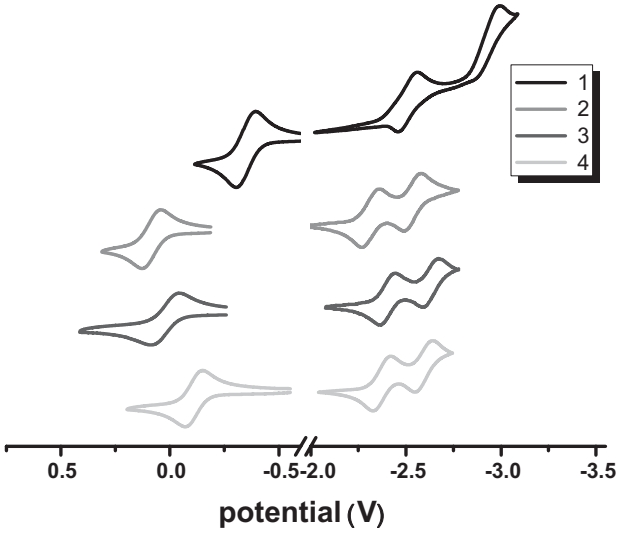

Figure 5. Cyclic voltammograms of Os(II) complexes **1**–**4**.

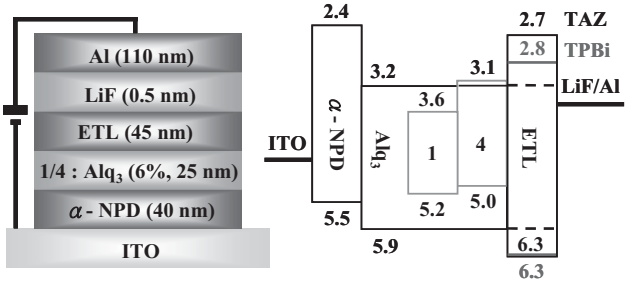

Figure 6. Device architecture and the estimated energy-level diagram of materials used in this work.

units and the phosphine (dppb vs. dmpb) may still exert some influence, but is much less significant than that imposed on the oxidative potentials. Finally, detection of dual reductions is attributed to the orthogonal arrangement and non-delocalized nature of N^N chelates in **2**–**4**; thus the second reduction will be strongly influenced by the preceding negative charge residing on the complex.[17]

2.4. Electroluminescence Properties of OLED Devices

NIR-emitting OLEDs based on complexes **1** and **4** were fabricated via vacuum thermal evaporation. The schematic device architecture and the estimated energy-level diagram of all materials used in this work are depicted in Figure 6. The device structure consists of: ITO/α-NPD (40 nm)/Alq_3, 6 wt % of dopant (25 nm)/ETL (45 nm)/LiF (0.5 nm)/Al (150 nm). *α*-NPD and Alq_3 represent 4,4′-bis[*N*-(1-naphthyl)-*N*-phenyl-amino]-biphenyl, and tris(8-hydroxyquinoline)aluminum, respectively. Alq_3 was chosen as the host material because its energy levels match well with both Os(II) dopants selected for the OLED investigations. Materials used for the electron transporting layer (ETL) include Alq_3, 2,2′,2″-(1,3,5-benzinetriyl)-tris(1-phenyl-1*H*-benzimidazole) (TPBi) and 3-(4-biphenylyl)-4-phenyl-5-(4-*tert*-butylphenyl)-1,2,4-triazole (TAZ), respectively. These ETL materials showed varied electron mobility,[18] distinctive HOMO/LUMO energy levels and triplet energies.[19] so that one may fine-tune and optimize device performances by varying ETL materials. The basic characteristics and performance data of all fabricated NIR-emitting OLEDs are summarized in Table 3.

Table 3. Basic characteristics and performance data of OLEDs fabricated using 6 wt % of **1** and **4**.

Device	1A	1B	1C	4A	4B	4C
ETL materials	Alq_3	TPBi	TAZ	Alq_3	TPBi	TAZ
Turn-on (V)	1.7	2.5	2.4	2.3	3.2	3.0
max. η_P ($lm\,W^{-1}$)	0.001	0.001	0.002	0.047	0.050	0.066
Max. EQE (%)	1.1	1.2	1.5	2.5	2.6	2.7
max. light output ($\mu W\,cm^{-2}$)[a]	55 (14)	64 (12)	65 (17)	120 (14)	172 (14)	93 (18)
EL λ_{max} (nm)	814	814	814	718	718	718

[a] Data in parentheses shows the operational voltage.

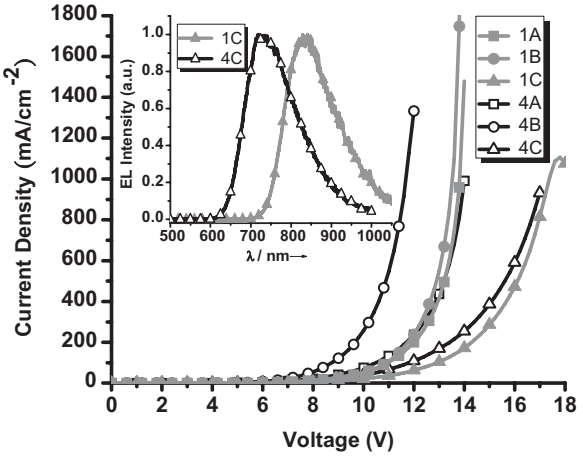

Figure 7. *I–V* characteristics for devices **1A**–**1C** and **4A**–**4C**; insert shows the normalized EL spectra of **1C** and **4C** recorded at driving voltage of 7 V.

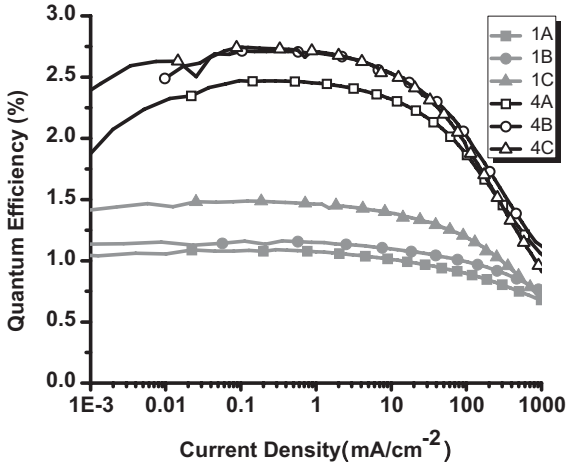

Figure 8. External quantum efficiencies of devices **1A**–**1C** and **4A**–**4C** with various electron transport layer(ETL) materials.

I–V curves of all devices are shown in Figure 7, for which the devices **A**, **B**, and **C** represent those fabricated using Alq_3, TPBi and TAZ as ETL for complexes **1** and **4**. Among all devices, 1B and 4B show the lowest operation voltage, while **1C** and **4C** show the highest operation voltage. Such difference in electrical characteristics is consistent with the electron-transport capability of the three ETL materials. For the electron mobility, TPBi is the fastest among three ETL materials while TAZ is the lowest.[16]

The inset of Figure 7 reveals the representative electroluminescence spectra of selected devices **1C** and **4C**, for which their emission profiles are consistent with the photoluminescence of each phosphor recorded in solution, confirming that the electroluminescence is derived from triplet excitons of the corresponding Os(II) complexes. Their EL peak wavelengths are located at 814 nm and 718 nm for **1** and **4**, respectively, and show negligible shift of emission wavelengths upon increasing voltage. The full width at half maximum (FWHM) for EL of **1** and **4** are 144 nm and 142 nm, respectively, which are greater than the FWHM of most Pt(II) based, NIR emitting phosphors.[11] The larger FWHM should be due to the lack of $\pi\pi$ stacking interaction existing in planar Pt(II) phosphors that may further strengthen the rigidity of the chelating chromophores.

It is notable that the devices of **1** and **4** using different ETL materials show rather different *I–V* characteristics (Fig. 7); however, the influences of different ETL materials on the EL efficiency are not significant (Fig. 8 and Table 3). For devices of **1**, the external quantum efficiencies (EQE) range from 1.1% to 1.5% photon/electron, while for devices of **4**, EQEs range from 2.5% to 2.7%. Moreover, the TAZ devices of both **1** and **4** show slightly higher EL quantum efficiencies of 1.5% and 2.7%. Since Alq_3 host itself is dominantly electron-transport, with the large enough triplet energy versus **1** and **4**, it can serve as an effective hole-blocking and exciton-confining material as well, rendering no appreciable difference in EL quantum efficiencies when using three different electron-transport/hole-blocking/exciton-confining materials. Nevertheless, using an ETL with a better electron-transport capability (e.g., TPBi) provides the benefit of reduced operational voltage.

Finally, one notices that the efficiency roll-off at high current densities, which is often observed in phosphorescent OLEDs, is not significant in these NIR devices fabricated by using both **1** and **4**. The EQEs of both series of devices remain rather constant up to high current densities of nearly 100 mA cm^{-2}. This may be associated with the intrinsic properties of both dopants, which have rather short excited-state lifetimes of 0.04 μs (**1**) and 0.16 μs (**4**), respectively in both device or in solid state. These lifetime values are significantly shorter than typical values of most phosphorescent complexes (on the order of μs or longer). The efficiency in roll-off is usually associated with the triplet-triplet annihilation under high populations of triplet excitons,[20] which in turn is associated with long excited-state lifetimes and thus ineffective relaxation pathways of most phosphorescent complexes. The shorter lifetime could reduce the population of the triplet excitons and thus substantially mitigate the triplet-triplet annihilation. With the reduced efficiency roll-off, the devices can be stably driven to high currents and high optical output. As such, forward radiant emittance as high as 65.02 μW cm^{-2} and 93.26 μW cm^{-2} can be reached at current densities of 931.5 mA cm^{-2} and 1075.8 mA cm^{-2} for devices of **1** and **4**, respectively.

3. Conclusions

In summary, this article presents a rational design for a new series of charge-neutral Os(II) complexes, which involves the usage of two isoquinolinyl triazolate chromophores and ancillary phosphine ligands, giving the corresponding NIR and deep-red emitting complexes. Employment of monodentate dimethylphenylphosphine afforded complex **1** with the *trans*-oriented triazolate chelates residing on the unique square plane, while reactions with chelating phosphines such as dppb and dmpb afforded the *cis*-isomers **2**–**4** that showed *trans*-arranged azolate fragments and *cis*-arranged isoquinolinyl fragments. Finally, complexes **1** and **4** exhibited the most efficient NIR and deep-red emission in solid state and were selected as a prototype for fabrication of

phosphorescent OLEDs using Alq_3 as the host, for which the maximum external quantum efficiencies are recorded to be as high as 1.5% and 2.7%, respectively. The OLEDs characterized in this work represents the only NIR-emitting devices fabricated using Os(II) phosphors up to this stage, while its non-ionic nature, intrinsic lower lying excited state, and relative short radiative lifetime are believed to be the key factors that gave this unprecedented achievement.

4. Experimental

General Information and Materials: Mass spectra were obtained on a JEOL SX-102A instrument operating in electron impact (EI) mode or fast atom bombardment (FAB) mode. ^{1}H and ^{13}C NMR spectra were recorded on Varian Mercury-400 or INOVA-500 instruments; chemical shifts are quoted with respect to the internal standard tetramethylsilane for ^{1}H and ^{13}C NMR data. Elemental analyses were carried out at the NSC Regional Instrumentation Center at National Chao Tung University, Hsinchu, Taiwan. The triazole chelates, namely: 5-(1-isoquinolyl)-3-*tert*-butyl-1,2,4-triazole (ibtz)H and 5-(1-isoquinolyl)-3-phenyl-1,2,4-triazole (iptz)H, were prepared according to the literature procedures [21]. All reactions were conducted under N_2 atmosphere using anhydrous solvents or solvents treated with an appropriate drying reagent.

Preparation of [Os(ibtz)$_2$(PPhMe$_2$)$_2$]: A mixture of $Os_3(CO)_{12}$ (150 mg, 0.16 mmol) and 5-(1-isoquinolyl)-3-*tert*-butyl-1,2,4-triazole (ibtzH, 267 mg, 1.06 mmol) in 30 mL of diethylene glycol methyl ether (DGME) was heated to 160 °C for 24 h. After cooled to room temperature, freshly sublimed Me_3NO (78 mg, 1.04 mmol) was added and the solution was then heated to ≈110 °C for 1 h, followed by addition of $PPhMe_2$ (144 mg, 1.04 mmol). After then, the solution was gradually heated to 180 °C and kept at this temperature for another 24 hours. Finally, the solvent was removed in vacuo to afford a tarry precipitate. Further purification was conducted by silica gel column chromatography (with a 1:3 mixture of ethyl acetate (EA) and hexane as eluent), followed by recrystallization from methanol at RT, giving a dark-brown crystalline solid [Os(ibtz)$_2$(PPhMe$_2$)$_2$] (**1**, 280 mg, 0.29 mmol) in 58% yield.

Spectral data of **1**: ^{1}H NMR (400 MHz, $CDCl_3$, 298 K, TMS: δ): 10.29 (d, J_{HH} = 6.4 Hz, 2H), 9.83 (dd, J_{HH} = 8.4, 0.8 Hz, 2H), 7.66 (d, J_{HH} = 8.4 Hz, 2H), 7.61–7.52 (m, 4H), 7.11 (d, J_{HH} = 6.4 Hz, 2H), 6.70(t, J_{HH} = 7.2 Hz, 2H), 6.59 (t, J_{HH} = 7.2 Hz, 4H), 6.25–6.21 (m, 4H), 1.64 (s, 18H), 0.75 (t, J_{HP} = 3.2 Hz, 6H), 0.54 (t, J_{HP} = 3.2 Hz, 6H); ^{31}P NMR (202 MHz, $CDCl_3$, 298K, TMS, δ): –22,14(s); MS (FAB, ^{192}Os): *m/z* 969 [M^+], 831 [M^+ – $PPhMe_2$]. Anal. calcd for $C_{46}H_{52}N_8OsP_2$: C 57.01, N 11.56, H 5.41; found: C 57.34, N 11.57, H 5.39.

Preparation of [Os(iptz)$_2$(dppb)]: Similar to the procedure described above for **1**, this reaction was conducted using $Os_3(CO)_{12}$ (70 mg, 0.08 mmol), 5-(1-isoquinolyl)-3-phenyl-1,2,4-triazole (iptzH, 130 mg, 0.48 mmol), Me_3NO (40 mg, 0.53 mmol) and dppb (120 mg, 0.27 mmol), giving the product [Os(iptz)$_2$(dppb)] (**2**, 68 mg, 0.06 mmol) in 25% yield.

Spectral data of **2**: ^{1}H NMR (400 MHz, d_6-acetone, 298K, TMS, δ): 10.11 (d, J_{HH} = 7.6 Hz, 2H), 8.22 (dd, J_{HH} = 8.0, 1.6 Hz, 4H), 8.06 (t, J_{HH} = 9.2 Hz, 4H), 7.75–7.66 (m, 8H), 7.54–7.47 (m, 6H), 7.42 (t, J_{HH} = 7.6 Hz, 2H), 7.38 (d, J_{HH} = 7.6 Hz, 2H), 7.35–7.31 (m, 4H), 7.23 (dd, J_{HH} = 6.8, 1.6 Hz, 2H), 7.18 (d, J_{HH} = 6.4 Hz, 2H), 6.82 (td, J_{HH} = 8.0, 1.6 Hz, 2H), 6.67–6.59 (m, 8H); ^{31}P NMR (202 MHz, d_6-acetone, 298 K, TMS, δ): 28.13 (s); MS (FAB, ^{192}Os): *m/z* 1181 [M^+]. Anal. calcd for $C_{64}H_{46}N_8OsP_2{\cdot}H_2O$: C 64.20, N 9.36, H 4.04; found: C 64.01, N 9.08, H 4.46.

Preparation of [Os(ibtz)$_2$(dppb)]: Similar to the procedure described above for **2**, this reaction was conducted using $Os_3(CO)_{12}$ (100 mg, 0.11 mmol), ibtzH (172 mg, 0.68 mmol), Me_3NO (57 mg, 0.77 mmol) and dppb (172 mg, 0.38 mmol), giving the product [Os(ibtz)$_2$(dppb)] (**3**, 169 mg, 0.15 mmol) in 45% yield.

Spectral data of **3**: ^{1}H NMR (500 MHz, d_6-acetone, 298 K, TMS, δ): 10.01 (d, J_{HH} = 8.8 Hz, 2H), 8.09 (t, J_{HH} = 8.8 Hz, 4H), 7.77–7.71 (m, 2H), 7.61–7.56 (m, 6H), 7.51–7.48 (m, 2H), 7.31 (t, J_{HH} = 7.0 Hz, 2H), 7.18 (t, J_{HH} = 6.8 Hz, 4H), 7.01 (dd, J_{HH} = 11.2, 6.4 Hz, 4H), 6.86 (t, J_{HH} = 6.4 Hz, 2H), 6.70–6.62 (m, 8H), 1.51 (s, 18H); ^{31}P NMR (202 MHz, d_6-acetone, 298 K, TMS, δ): 27.64 (s); MS (FAB, ^{192}Os): *m/z* 1141 [$M + 1$]$^+$. Anal. calcd for $C_{60}H_{54}N_8OsP_2$: C 63.25, N 9.84, H 4.78; found: C 62.87, N 9.62, H 5.07.

Preparation of [Os(ibtz)$_2$(dmpb)]: Similar to the procedure described above for **2**, this reaction was conducted using $Os_3(CO)_{12}$ (100 mg, 0.11 mmol), ibtzH (178 mg, 0.71 mmol), Me_3NO (50 mg, 0.67 mmol) and 1,2-bis(dimethylphosphino)benzene (dmpb, 80 mg, 0.40 mmol), giving the desired product [Os(ibtz)$_2$(dmpb)] (**4**, 65 mg, 0.07 mmol) in 22% yield.

Spectral data of **4**: ^{1}H NMR (400 MHz, d_6-acetone, 298 K, TMS, δ): 10.32–10.26 (m, 2H), 7.98–7.91 (m, 2H), 7.82–7.78 (m, 2H), 7.76–7.69 (m, 4H), 7.58–7.50 (m, 2H), 7.42–7.35 (m, 4H), 2.16 (d, J_{HP} = 10.0 Hz, 6H), 1.45 (s, 18H), 0.65 (d, J_{HP} = 8.8 Hz, 6H); ^{31}P NMR (202 MHz, d_6-acetone, 298 K, TMS, δ): 8.92 (s); MS (FAB, ^{192}Os): *m/z* 892 [$M + 1$]$^+$. Anal. calcd for $C_{40}H_{46}N_8OsP_2$: C 53.93, N 12.58, H 5.20; found: C 53.88, N 12.12, H 5.38.

Selected crystal data of **4**: $C_{41}H_{50}N_8OOsP_2$, M = 923.03, monoclinic, space group $P\,2_1/c$, T = 150(2) K, a = 20.5611(12), b = 11.7661(7), c = 17.5029(11) Å, β = 111.515(1)°, V = 3939.3(4) Å^3, Z = 4, ρ_{calcd} = 1.556 mg m^{-3}, $F(000)$ = 1864, λ(Mo Kα) = 0.7107 Å, μ = 3.362 mm^{-1}, crystal size = 0.32 × 0.25 × 0.08 mm^3, 9047 independent reflections collected (R_{int} = 0.0438), GOF = 1.050, final $R_1[I > 2\sigma(I)]$ = 0.0291, wR_2(all data) = 0.0612, and D-map, max./min. = 1.286/−1.161 e/Å^3. The crystallographic data (excluding structure factors) has been deposited in the Cambridge Crystallographic Data Centre with the deposition number CCDC-721890. This data can be obtained free of charge on application to CCDC, 12 Union Road, Cambridge CB21EZ, UK (fax: (+44) 1223-336-033; e-mail: deposit@ccdc.cam.ac.uk).

X-Ray Diffraction Studies: Single crystal X-ray diffraction data were measured on a Bruker SMART Apex CCD diffractometer using (Mo-K$_\alpha$) radiation (λ = 0.71073 Å). The data collection was executed using the SMART program. Cell refinement and data reduction were performed with the SAINT program. The structure was determined using the SHELXTL/PC program and refined using full-matrix least squares.

Electrochemical Measurement: Cyclic voltammetry (CV) measurements were performed using a BAS 100 B/W electrochemical analyzer. The oxidation and reduction measurements were recorded using Pt wire and Au disks coated with Hg as working electrodes, respectively, in anhydrous CH_2Cl_2 and THF solution containing 0.1 M $TBAPF_6$ as the supporting electrolyte, at the typical scan rate of 100 mV s^{-1}. The potentials were measured against an Ag/Ag^+ (0.01 M $AgNO_3$) reference electrode with ferrocene as the internal standard (0.53 V).

Photophysical Data Measurement and OLED Fabrication: Steady-state absorption, emission, and phosphorescence lifetime measurements both in solution and in the solid state have been described in our previous reports [22]. The fabrication procedures for the OLED devices including those for patterning and cleaning of ITO substrates followed those described in the literature [23]. The multilayer device was fabricated by thermal evaporation in a vacuum chamber with a base pressure of ≤10^{-6} Torr, as well as in a single pump-down without breaking vacuum. The deposition rate was kept at ≈0.2 nm s^{-1}. The active area of the device is 1 × 1 mm^2, as defined by the shadow mask for cathode deposition. The current-voltage-brightness (*I–V–L*) characteristics of devices were measured using an Agilent 4155B semiconductor parameter analyzer and a Si photodiode calibrated with Photo Research PR-650 spectrometer. The hole transporting, host matrix, hole blocking and electron transporting materials was selected according to their relative energy levels, which are obtained from those reported in literature and extracted from our CV measurements [17].

Computational Methodology: Calculations on the electronic first triplet state of complexes **1**–**4** were carried out using B3LYP density functional theory [24]. A "double-ζ" quality basis set consisting of Hay and Wadt's effective core potentials (LANL2DZ) [25] was employed for Os atom, and a 6-31G* basis [26] for H, C, N, and P atoms. A relativistic effective core potential (ECP) replaced the inner core electrons of Os(II), leaving the outer core (5s^{2}5p^6) electrons and the 5d^6 valence electrons. Time-dependent DFT (TDDFT) calculations using the B3LYP functional were then performed on the basis of the structural optimized geometries [27].

Typically, the lowest triplet root of the nonhermitian eigenvalue equations was obtained to determine the vertical excitation energies. The first triplet state B3LYP and excited-state TDDFT calculations were carried out using Gaussian03 [28].

Compositions of molecular orbitals in terms of the constituent chemical fragments were calculated using the AOMix program [29]. For the characterization of the HOMO–$x \rightarrow$ LUMO+y transitions as partial charge transfer (CT) transitions, the following definition of the CT character was used:

$$\mathrm{CT(M)} = \%(\mathrm{M})\mathrm{HOMO} - x - \%(\mathrm{M})\mathrm{LUMO} + y \quad (1)$$

where %(M)HOMO–x and %(M)LUMO+y are electronic densities on the metal in HOMO–x and LUMO+y. If the excited state, e.g., S_1 or T_1, is formed by more than one one-electron excitation, then the metal CT character of this excited state is expressed as a sum of CT characters of each participating excitation, $i \rightarrow j$:

$$\mathrm{CT_I(M)} = \sum_{i,a} [C_I(i \rightarrow j)]^2 (\%(\mathrm{M})_i - \%(\mathrm{M})_j) \quad (2)$$

where C_I ($i \rightarrow j$) are the appropriate coefficients of the I-th eigenvector of the CI matrix. Accordingly, one can very effectively use the MO compositions in terms of fragment orbital contributions to probe the nature of electronic transitions.

Acknowledgements

We thank the National Science Council of Taiwan, for the financial supports (NSC 93-2113-M-007-012) and (NSC 93-ET-7-007-003).

Received: February 9, 2009
Revised: March 4, 2009
Published online: July 1, 2009

[1] a) M. A. Baldo, D. F. O'Brien, Y. You, A. Shoustikov, S. Sibley, M. E. Thompson, S. R. Forrest, *Nature* **1998**, *395*, 151. b) S. Welter, K. Brunner, J. W. Hofstraat, L. De Cola, *Nature* **2003**, *421*, 54. c) H. Yersin, *Top. Curr. Chem.* **2004**, *241*, 1. d) E. Holder, B. M. W. Langeveld, U. S. Schubert, *Adv. Mater.* **2005**, *17*, 1109. e) R. C. Evans, P. Douglas, C. J. Winscom, *Coord. Chem. Rev.* **2006**, *250*, 2093.

[2] T. Fuhrmann, J. Salbeck, *MRS Bull.* **2003**, *28*, 354.

[3] C.-F. Chang, Y.-M. Cheng, Y. Chi, Y.-C. Chiu, C.-C. Lin, G.-H. Lee, P.-T. Chou, C.-C. Chen, C.-H. Chang, C.-C. Wu, *Angew. Chem.* **2008**, *120*, 4618; *Angew. Chem. Int. Ed.* **2008**, *47*, 4542.

[4] M. K. Nazeeruddin, R. Humphry-Baker, D. Berner, S. Rivier, L. Zuppiroli, M. Graetzel, *J. Am. Chem. Soc.* **2003**, *125*, 8790.

[5] Y.-S. Yeh, Y.-M. Cheng, P.-T. Chou, G.-H. Lee, C.-H. Yang, Y. Chi, C.-F. Shu, C.-H. Wang, *ChemPhysChem* **2006**, *7*, 2294.

[6] a) Y.-C. Chiu, J.-Y. Hung, Y. Chi, C.-C. Chen, C.-H. Chang, C.-C. Wu, Y.-M. Cheng, Y.-C. Yu, G.-H. Lee, P.-T. Chou, *Adv. Mater.* **2009**, *21*, 2221. b) Y.-C. Chiu, Y. Chi, J.-Y. Hung, Y.-M. Cheng, Y.-C. Yu, M.-W. Chung, G.-H. Lee, P.-T. Chou, C.-C. Chen, C.-C. Wu, H.-Y. Hsieh, *ACS Appl. Mater. Int.* **2009**, *1*, 433.

[7] a) D. R. Gamelin, H. U. Guedel, *Acc. Chem. Res.* **2000**, *33*, 235. b) J.-C. G. Buenzli, C. Piguet, *Chem. Soc. Rev.* **2005**, *34*, 1048. c) M. I. J. Polson, F. Loiseau, S. Campagna, G. S. Hanan, *Chem. Commun.* **2006**, 1301.

[8] a) G. Qian, B. Dai, M. Luo, D. Yu, J. Zhan, Z. Zhang, D. Ma, Z. Y. Wang, *Chem. Mater.* **2008**, *20*, 6208. b) Y. Yang, R. T. Farley, T. T. Steckler, S.-H. Eom, J. R. Reynolds, K. S. Schanze, J. Xue, *Appl. Phys. Lett.* **2008**, *93*, 163305.

[9] a) H.-Y. Chen, C.-H. Yang, Y. Chi, Y.-M. Cheng, Y.-S. Yeh, P.-T. Chou, H.-Y. Hsieh, C.-S. Liu, S.-M. Peng, G.-H. Lee, *Can. J. Chem.* **2006**, *84*, 309. b) E. L. Williams, J. Li, G. E. Jabbour, *Appl. Phys. Lett.* **2006**, *89*, 083506.

[10] a) C.-J. Yang, C. Yi, M. Xu, J.-H. Wang, Y.-Z. Liu, X.-C. Gao, J.-W. Fu, *Appl. Phys. Lett.* **2006**, *89*, 233506. b) C. Borek, K. Hanson, P. I. Djurovich, M. E. Thompson, K. Aznavour, R. Bau, Y. Sun, S. R. Forrest, J. Brooks, L. Michalski, J. Brown, *Angew. Chem.* **2007**, *119*, 1127; *Angew. Chem. Int. Ed.* **2007**, *46*, 1109. c) M. Cocchi, D. Virgili, V. Fattori, J. A. G. Williams, J. Kalinowski, *Appl. Phys. Lett.* **2007**, *90*, 023506. d) M. Cocchi, J. Kalinowski, D. Virgili, J. A. G. Williams, *Appl. Phys. Lett.* **2008**, *92*, 113302. e) H.-F. Xiang, Z.-X. Xu, V. A. L. Roy, B.-P. Yan, S.-C. Chan, C.-M. Che, P. T. Lai, *Appl. Phys. Lett.* **2008**, *92*, 163305. f) T. C. Rosenow, K. Walzer, K. Leo, *J. Appl. Phys.* **2008**, *103*, 043105.

[11] Y. Sun, C. Borek, K. Hanson, P. I. Djurovich, M. E. Thompson, J. Brooks, J. J. Brown, S. R. Forrest, *Appl. Phys. Lett.* **2007**, *90*, 213503.

[12] a) P.-T. Chou, Y. Chi, *Chem. Eur. J.* **2007**, *13*, 380. b) Y. Chi, P.-T. Chou, *Chem. Soc. Rev.* **2007**, *36*, 1421. c) P.-T. Chou, Y. Chi, *Eur. J. Inorg. Chem.* **2006**, 3319.

[13] a) J. Yang, A. Dass, C. Sotiriou-Leventis, D. S. Tyson, N. Leventis, *Inorg. Chim. Acta* **2005**, *358*, 389. b) S. Wang, X. Li, S. Xun, X. Wan, Z. Y. Wang, *Macromolecules* **2006**, *39*, 7502.

[14] a) Y. L. Tung, P. C. Wu, C. S. Liu, Y. Chi, J. K. Yu, Y. H. Hu, P. T. Chou, S. M. Peng, G. H. Lee, Y. Tao, A. J. Carty, C. F. Shu, F. I. Wu, *Organometallics* **2004**, *23*, 3745. b) Y.-L. Tung, S.-W. Lee, Y. Chi, Y.-T. Tao, C.-H. Chien, Y.-M. Cheng, P.-T. Chou, S.-M. Peng, C.-S. Liu, *J. Mater. Chem.* **2005**, *15*, 460.

[15] a) Y.-L. Tung, S.-W. Lee, Y. Chi, L.-S. Chen, C.-F. Shu, F.-I. Wu, A. J. Carty, P.-T. Chou, S.-M. Peng, G.-H. Lee, *Adv. Mater.* **2005**, *17*, 1059. b) Y. L. Tung, L. S. Chen, Y. Chi, P. T. Chou, Y. M. Cheng, E. Y. Li, G. H. Lee, C. F. Shu, F. I. Wu, A. J. Carty, *Adv. Funct. Mater.* **2006**, *16*, 1615.

[16] a) Y.-L. Chen, C. Sinha, I.-C. Chen, K.-L. Liu, Y. Chi, J.-K. Yu, P.-T. Chou, T.-H. Lu, *Chem. Commun.* **2003**, 3046. b) Y.-M. Cheng, E. Y. Li, G.-H. Lee, P.-T. Chou, S.-Y. Lin, C.-F. Shu, K.-C. Hwang, Y.-L. Chen, Y.-H. Song, Y. Chi, *Inorg. Chem.* **2007**, *46*, 10276. c) K.-C. Hwang, J.-L. Chen, Y. Chi, C.-W. Lin, Y.-M. Cheng, G.-H. Lee, P.-T. Chou, S.-Y. Lin, C.-F. Shu, *Inorg. Chem.* **2008**, *47*, 3307.

[17] a) I.-S. Shin, J. I. Kim, T.-H. Kwon, J.-I. Hong, J.-K. Lee, H. Kim, *J. Phys. Chem. C* **2007**, *111*, 2280. b) A. Kapturkiewicza, J. Nowackib, P. Borowicza, *Electrochim. Acta* **2005**, *50*, 3395.

[18] a) R. G. Kepler, P. M. Beeson, S. J. Jacobs, R. A. Anderson, M. B. Sindair, V. S. Valencia, P. A. Cahil, *Appl. Phys. Lett.* **1995**, *66*, 3618. b) T. Yasuda, Y. Yamaguchi, D.-C. Zou, T. Tsutsui, *Jpn. J. Appl. Phys. Part 1* **2002**, *41*, 5626. c) W.-Y. Hung, T.-H. Ke, Y.-T. Lin, C.-C. Wu, T.-H. Hung, T.-C. Chao, K.-T. Wong, C.-I. Wu, *Appl. Phys. Lett.* **2006**, *88*, 064102.

[19] a) H. Fukagawa, K. Watanabe, T. Tsuzuki, S. Tokito, *Appl. Phys. Lett.* **2008**, *93*, 133312. b) M.-H. Tsai, H.-W. Lin, H.-C. Su, C.-C. Wu, F.-C. Fang, Y.-L. Liao, K.-T. Wong, C.-I. Wu, *Adv. Mater.* **2006**, *18*, 1216. c) I. Tanaka, S. Tokito, *J. Appl. Phys.* **2005**, *97*, 113532. d) S.-H. Kim, J. Jang, K.-S. Yook, J.-Y. Lee, M.-S. Gong, S. Ryu, G.-K. Chang, H.-J. Chang, *J. Appl. Phys.* **2008**, *103*, 054502. e) G. He, M. Pfeiffer, K. Leo, M. Hofmann, J. Birnstock, R. Pudzich, J. Salbeck, *Appl. Phys. Lett.* **2004**, *85*, 3911.

[20] a) M. A. Baldo, C. Adachi, S. R. Forrest, *Phys. Rev. B* **2000**, *62*, 10967. b) R. G. Kepler, J. C. Caris, P. Avakian, E. Abramson, *Phys. Rev. Lett.* **1963**, *10*, 400. c) V. Ern, H. Bouchriha, J. Fourny, G. Delacote, *Solid State Commun.* **1971**, *9*, 1201.

[21] a) K. Funabiki, N. Noma, G. Kuzuya, M. Matsui, K. Shibata, *J. Chem. Res. Miniprint* **1999**, 1301. b) R. Hage, R. Prins, J. G. Haasnoot, J. Reedjik, *J. Chem. Soc. Dalton Trans.* **1987**, 1389.

[22] P. T. Chou, W. S. Yu, Y. M. Cheng, S. C. Pu, Y. C. Yu, Y. C. Lin, C. H. Huang, C. T. Chen, *J. Phys. Chem. A* **2004**, *108*, 6487.

[23] C.-H. Yang, Y.-M. Cheng, Y. Chi, C.-J. Hsu, F.-C. Fang, K.-T. Wong, P.-T. Chou, C.-H. Chang, M.-H. Tsai, C.-C. Wu, *Angew. Chem.* **2007**, *119*, 2470; *Angew. Chem. Int. Ed.* **2007**, *46*, 2418.

[24] a) C. Lee, W. Yang, R. G. Parr, *Phys. Rev. B* **1988**, *37*, 785. b) A. D. Becke, *J. Chem. Phys.* **1993**, *98*, 5648.

[25] a) P. J. Hay, W. R. Wadt, *J. Chem. Phys.* **1985**, *82*, 270. b) W. R. Wadt, P. J. Hay, *J. Chem. Phys.* **1985**, *82*, 284. c) P. J. Hay, W. R. Wadt, *J. Chem. Phys.* **1985**, *82*, 299.

[26] P. C. Hariharan, J. A. Pople, *Mol. Phys.* **1974**, *27*, 209.

[27] a) C. Jamorski, M. E. Casida, D. R. Salahub, *J. Chem. Phys.* **1996**, *104*, 5134. b) M. Petersilka, U. J. Grossmann, E. K. U. Gross, *Phys. Rev. Lett.* **1996**, *76*, 1212. c) R. Bauernschmitt, R. Ahlrichs, F. H. Hennrich, M. M. Kappes, *J. Am. Chem. Soc.* **1998**, *120*, 5052. d) M. E. Casida, *J. Chem. Phys.* **1998**, *108*, 4439. e) R. E. Stratmann, G. E. Scuseria, M. J. Frisch, *J. Chem. Phys.* **1998**, *109*, 8218.

[28] *Gaussian 03*, Revision C.02, M. J. Frisch, G. W. Trucks, H. B. Schlegel, G. E. Scuseria, M. A. Robb, J. R. Cheeseman, J. A. Montgomery, Jr, T. Vreven, K. N. Kudin, J. C. Burant, J. M. Millam, S. S. Iyengar, J. Tomasi, V. Barone, B. Mennucci, M. Cossi, G. Scalmani, N. Rega, G. A. Petersson, H. Nakatsuji, M. Hada, M. Ehara, K. Toyota, R. Fukuda, J. Hasegawa, M. Ishida, T. Nakajima, Y. Honda, O. Kitao, H. Nakai, M. Klene, X. Li, J. E. Knox, H. P. Hratchian, J. B. Cross, V. Bakken, C. Adamo, J. Jaramillo, R. Gomperts, R. E. Stratmann, O. Yazyev, A. J. Austin, R. Cammi, C. Pomelli, J. W. Ochterski, P. Y. Ayala, K. Morokuma, G. A. Voth, P. Salvador, J. J. Dannenberg, V. G. Zakrzewski, S. Dapprich, A. D. Daniels, M. C. Strain, O. Farkas, D. K. Malick, A. D. Rabuck, K. Raghavachari, J. B. Foresman, J. V. Ortiz, Q. Cui, A. G. Baboul, S. Clifford, J. Cioslowski, B. B. Stefanov, G. Liu, A. Liashenko, P. Piskorz, I. Komaromi, R. L. Martin, D. J. Fox, T. Keith, M. A. Al-Laham, C. Y. Peng, A. Nanayakkara, M. Challacombe, P. M. W. Gill, B. Johnson, W. Chen, M. W. Wong, C. Gonzalez, J. A. Pople, Gaussian, Inc, Wallingford, CT **2004**.

[29] a) S. I. Gorelsky, *AOMix: Program for Molecular Orbital Analysis*, http://www.sg-chem.net/, University of Ottawa, Ottawa **2007**. b) S. I. Gorelsky, A. B. P. Lever, *J. Organomet. Chem.* **2001**, *635*, 187.